Accepted manuscript doi:
10.1680/jgein.23.00178

Submitted: 22 November 2023

Published online in 'accepted manuscript' format: 29 March 2024

Manuscript title: Long-term performance of HDPE extrusion Welds aged at 85°C in synthetic leachate

Authors: M. Ali and R. K. Rowe

Affiliation: GeoEngineering Centre at Queen's – RMC, Department of Civil Engineering, Queen's University, Kingston, Canada

Corresponding author: R. K. Rowe, GeoEngineering Centre at Queen's – RMC, Department of Civil Engineering, Queen's University, Kingston, Canada, K7L 3N6.

E-mail: kerry.rowe@queensu.ca

Accepted manuscript doi:
10.1680/jgein.23.00178

Abstract

The effect of ageing at 85°C of extrusion welds of 1.5 mm-thick high-density polyethylene (HDPE) geomembrane, immersed in synthetic municipal solid waste leachate, is investigated with respect to its standard oxidative induction time (Std-OIT) and stress crack resistance (SCR). Results show that the heat-affected zones (HAZ) adjacent to the squeeze-out bead (flashing) may exhibit faster STD-OIT depletion than the sheet. Generally, individual weld SCR failure times were observed to be between that of the notched and unnotched sheet. Welds with high welding-induced geometric irregularities (WIGI), and overheated fusion and extrusion welds are shown to result in SCR failure times close to that of a notched sheet during immersion time. The average time to nominal failure (taken to be when t_{NF} =250 hours) of Cool and Good welding parameter combinations ranges between 3% and 15% shorter than the unnotched sheet. Differences in t_{NF} were attributed to accelerated craze formation in welds with high WIGI from stress concentration. No significant difference was observed between the SCR values of fusion and extrusion welds during 40 months of immersion in MSW-L3. This paper shows that overgrind negatively impacts the SCR of welds and accelerates the degradation of SCR.

Keywords: geosynthetics, extrusion welds, fusion welds, ageing, long-term performance, stress cracking resistance, HDPE, geomembranes, quality assurance

Accepted manuscript doi:
10.1680/jgein.23.00178

1. INTRODUCTION

High-density polyethylene geomembranes (HDPE) are used as part of barrier systems in different geoenvironmental applications to provide containment to fluids such as landfill leachate, tailing fluids, and others (Hsuan and Koerner 1998; Scheirs 2009; Abdelaal et al. 2019; Di Battista and Rowe 2020; Morsy and Rowe 2020; Francey and Rowe 2022b; Francey and Rowe 2023). The service life of the geomembrane is a function of sheet resistance to ageing, stress due to indentions or wrinkles, geomembrane thickness, chemical composition of the in-contact leachate, adjacent materials, and temperature (Hsuan and Koerner 1998; Tognon et al. 2000; Sangam and Rowe 2005; Take rt al. 2007; Scheirs 2009, Rowe and Islam 2009; Rowe et al 2010a,b; Rowe and Yu 2019). When exposed to chemicals and elevated temperatures, geomembranes can exhibit chemical degradation, leading to a loss of their mechanical properties. This degradation occurs in three conceptual stages (Hsuan and Koerner 1998). Stage I: the antioxidants present in the geomembrane are slowly consumed or diffused out of the geomembrane. Despite this, they still provide protection from oxidative degradation and prevent a reduction in mechanical properties, except for those related to morphological changes and physical ageing (Ewais and Rowe 2014; Rowe et al. 2019). Stage II represents the induction time during which free radical species accumulate within the geomembrane microstructure. Stage III starts when polymer degradation occurs, leading to significant changes in the geomembrane's physical and mechanical properties, such as stress crack resistance (SCR; ASTM (D5397)), Melt Flow Rate (MFR; ASTM (D1238)), and tensile property (ASTM D6693). The time to nominal failure (t_{NF}) is reached when the geomembrane loses 50% of a certain reference value. The reference value is a subject of some debate. Historically, it has most commonly been taken as either the initial or the specified SCR value (Seeger and Muller 2003).

Stress cracking may occur when the geomembrane is subjected to stresses lower than its yield strength (ASTM D5397). Thus, most barrier system designs suggest limiting the applied stresses to a value lower than the geomembrane's yield strength (Hsuan 2000; Rowe and Sangam 2002). However, several factors can lead to premature brittle failures, such as gravel indentations, geomembrane wrinkles, down drag resulting from side slopes, thermal contraction, poor construction, differential settlement, and welds (Peggs and Carlson 1990a; Chappel et al. 2012; Abdelaal et al. 2014b; Ewais et al. 2014; Francey and Rowe 2022a).

HDPE geomembranes are used as rolled sheets and require welding to form an impermeable seal layer. There are two common methods for welding HDPE geomembranes: fusion welding and extrusion welding. Fusion welding is used for welding panel overlaps and serves as the primary technique for creating the majority of the weld length in the geomembrane barrier system (Scheirs 2009). Meanwhile, extrusion welding is primarily used to weld patches, panel intersections, and to

repair defects in HDPE geomembrane sheets (Seeger and Muller 2003; Touze-Foltz et al. 2008; Scheirs 2009). Extrusion welds require a skilled operator and pre-weld preparation, such as removing dirt, controlling welding pressure, and adequately grinding the sheet surface. Extrusion welding is a manual technique, and excessive pressure by the welder can cause welding-induced geometric irregularities (WIGI), leading to increased stresses across the weld. Grinding is essential to remove oxidized layers and additive bloom. However, improper grinding (over-grinding) increases strain/stress concentrations and can potentially lead to stress cracking in the field (Scheirs 2009; Toepfer 2015; Rowe and Ali 2024). Such issues were observed by Rowe et al. (1998) in a 14-year-old geomembrane used as a liner for a leachate lagoon. Hsuan (2000) also observed stress cracking in HDPE geomembranes extracted from 16 sites. They suggested that the majority of the cracking was associated with exposed geomembranes and primarily occurred at weld patches, scratches, and overlapped welds where stress concentrations were present. High welding temperatures (overheating) can also cause stress cracking. For instance, Hsuan (2000) observed slow and rapid stress cracks at 16 different sites, arguing that these occurred due to overheating and/or overgrinding. Rowe and Ali (2024) examined the effect of over-grinding on the SCR of a 1.5 mm unaged HDPE geomembrane extrusion weld. They found that the overground surface reduced the unnotched SCR by 99% compared to the best extrusion welds. Extrusion welds with high WIGI reduced the unnotched SCR to only about 9% of that of the unnotched sheet. These observations raise questions about the effects of WIGI and over-grinding on the long-term behavior of the extrusion weld. This paper addresses those questions.

It's a common perception that extrusion welding is inferior to fusion welding. For instance, Gilson-Beck and Giroud (2022) compared the leak frequency per unit seam length for fusion and extrusion welds by analyzing the electrical leak location (ELL) test results from 35 projects. They concluded that the leak frequency associated with extrusion welds was 60 to 100 times that of those associated with fusion welds. Rowe and Ali (2024) showed that factors such as high WIGI and overgrinding can significantly affect the SCR value of extrusion welds. However, they found no statistically significant difference between high-quality extrusion and fusion welds. This suggests that extrusion welding isn't inherently inferior but can easily become problematic with inadequate quality control (QC). Thus, Gilson-Beck and Giroud (2022) were justified when they suggested minimizing extrusion welds and avoiding long extrusion welds, which can lead to operator fatigue and increase the possibility of defects.

HDPE geomembranes commonly contain additives, such as antioxidants and carbon black, to enhance their protection during manufacturing and installation (Hsuan and Koerner 1998; Scheirs 2009; Abdelaal et al. 2019; Morsy and Rowe 2020; Francey and Rowe 2022a; Francey and Rowe 2023). Antioxidants serve as oxidation buffers for the polymer. Over time, these antioxidants slowly

Accepted manuscript doi:
10.1680/jgein.23.00178

oxidize or diffuse out of the geomembrane during its operation to extend the service life (Hsuan 2000; Rowe and Sangam 2002). Fusion welds may exhibit pre-aged partial antioxidant depletion during welding within their heat-affected zones (HAZs). The HAZ is a section of the weld exposed to high temperatures and has a thickness equal to that of the sheet material (Rowe and Shoaib 2017; Zhang et al. 2017; Rowe and Shoaib 2018). The unaged standard oxidative induction time (Std-OIT) of the HAZ of an extrusion weld is similar to that of the sheet (Rowe and Ali 2024). The longevity effect of fusion welds was examined by Francey and Rowe (2022a) by immersing the welds in simulated landfill leachate at 85°C. They showed that the antioxidant (AO) depletion rate of the HAZ of fusion welds exhibited similar behaviour to that of the sheet. The welding parameter combinations showed negligible effect on the AO depletion rate (Francey and Rowe 2022a). Except for Ali and Rowe (2023), there are no published studies of the long term performance of extrusion welds. Ali and Rowe (2023) immersed extrusion welds in simulated municipal solid waste landfill leachate (MSW-L3) at 85°C. They found that the antioxidant depletion rate of the extrudate bead was slower than that of the sheet at 85°C and they attributed this to the greater thickness of the bead zone and the higher Std-OIT of the welding rod used. They observed a faster Std-OIT depletion rate in the extrudate bead at a lower temperature (i.e. 65°C , which resulted in a predicted difference of an order of magnitude in the time to antioxidant depletion at 35°C from 3.9 years for the bead and 40 years for the sheet away from the weld. This suggests that polymer degradation, resulting from high welding temperatures, becomes more apparent at lower temperatures. Thus, in view of the paucity of research investigating the long-term performance of the extrusion weld, the objective of this paper is to:

1. Examine the effect of extrusion welding temperatures on the antioxidant depletion rate.
2. Evaluate the impact of weld bead geometry irregularity and over-grind extrusion welding on the SCR degradation with incubation time.
3. Compare the long-term behavior of SCR between HDPE geomembrane extrusion welds and fusion welds.

2. Materials and methods

2.1 Geomembrane

One 1.5mm HDPE flat die geomembrane (denoted as MwA-15) was examined (Table 1). MwA15 was manufactured in 2011. The unaged Std-OIT_o was 162 ± 4min, HP-OIT_o was 1320 ± 12min, SCR_o (ASTM D5397) was 1080 ± 83 hours, all of them exceed the requirements of GRI-GM13.

Accepted manuscript doi:
10.1680/jgein.23.00178

2.2 Welding Procedure

The geomembrane surfaces were cleaned and ground to remove any oxidized surface and waxy layers (Scheirs 2009; Toepfer 2015). The extrusion welds were created using a Demtech extrusion welder by an experienced welding technician on a summer day when the sheet temperature was 37 °C. The top and bottom geomembrane sheets were preheated with hot air (to a temperature T_p that was higher than the geomembrane's melting point) to reduce the amount of welding heat required, increase the size of the extrudate bead and avoid thermal shock, which can cause a weakening in the polymeric structure at the edge of the welding bead (Mollard et al. 1996). The welding rod, made from the same resin as the geomembrane, was melted inside the barrel (to a temperature of T_e) and then pushed out through the nozzle, taking the shape of the Teflon shoe, and adhered to the geomembranes to form the weld (Scheirs 2009; Toepfer 2015). The welds were left exposed to the sun to allow cooling naturally in the sun before transport to the laboratory and stored at 21°C.

Three welding parameter combinations were examined, denoted as "overheated", "Good", and "Cool". The high heat "Overheated" cases had a preheat temperature T_p = 277°C and barrel temperature T_e = 288°C. The "Good" weld cases had T_p = 220°C and T_e = 230°C. The "Cool" welding cases had T_p =150°C and T_e = 230°C.

2.3 Standard Oxidative Induction Time (Std-OIT)

Standard oxidative induction time (Std-OIT) (35kPa/200 °C; ASTM (D3895)) was conducted to monitor the depletion of the antioxidant packages in the geomembrane and welds. The Std-OIT specimens, approximately 5 mg, were prepared by cutting from five locations (Figure 1) on the welded specimens.

The unaged Std-OIT value was used as a baseline from which the rate of antioxidant depletion rate was measured and compared. This depletion rate was calculated using a first-order (exponential) decay model (Hsuan and Koerner 1998):

$$\text{Std-OIT}_t = \text{Std-OIT}_o\, e^{-st} \qquad (2)$$

where Std-OIT_t (min) is the Std-OIT value at a time (t), Std-OIT_o is the initial Std-OIT value, *s* is the antioxidant depletion rate (month^{-1}), and t is the incubation time (month).

2.4 Melt Flow Index (MFI)

The melt flow index (MFI) tests (ASTM D1238) were conducted to infer the change in the polymer's molecular weight, which is associated with cross-linking and/or chain-scission degradation (Hsuan and Koerner 1998).

2.5 Stress Crack Resistance Testing (SCR)

Stress crack resistance (SCR) testing was performed on notched sheets ((ASTM D5397), (GRI-GM 5(c)), unnotched sheets and unnotched welds. SCR tests were conducted on unnotched welds by centring the heat-affected zone within the center parallel region of the specimens. Both notched and unnotched specimens were immersed in a 10% Igepal solution at 50°C and subjected to a constant tensile load equal to 30% of the sheet's yield strength for their corresponding cross-sectional area.

The unnotched weld SCR testing is considered a more reliable testing metric for assessing the SCR of HDPE geomembrane than the notched welds because it better simulates field loading conditions (Francey and Rowe 2022b; Rowe and Ali 2024). The absence of the notch allows the welds to crack at locations most likely to occur in the field. Consequently, crack initiation and propagation start at the HAZ adjacent to the squeeze-out bead (flashing), extending towards the opposing sheet face. This allows the material adjacent to the flashing to fall within the specimen's brittle detachment zone. Thus, the unnotched weld SCR test is considered the preferred method for evaluating HDPE geomembrane welds (Francey and Rowe 2022b; Francey and Rowe 2022a; Rowe and Ali 2024).

2.6 Shear Test

Shear strength tests were performed in accordance with ASTM (D6392) using a Zwick Roell (Model Z020) machine at a strain rate of 50mm/min. Weld specimens were cut perpendicular to the weld, with dimensions of 150 mm long by 25 mm wide.

2.7 Immersion Test

The geomembrane coupons (19 cm × 10 cm) from the sheets and welds were immersed in 4-litre glass jars filled with simulated synthetic municipal solid waste leachate (denoted as MSW-L3). The chemical components of the synthetic leachate (Table 2) were chosen based on the chemical analysis of the Keele Valley landfill in Ontario, Canada (Rowe et al. 2008; Abdelaal et al. 2014b), including organic/inorganic salts, surfactant, and trace metal solution mixed in reduced conditions (electrical potential Eh ≈ -120 mV; 12,000mg/L and pH≈7). The geomembrane coupons were separated using 5mm diameter glass rods to allow the coupons to be exposed from both sides.

3. Results and Discussion

3.1 Std-OIT depletion

Std-OIT depletion was examined for the sheet material and three welding parameter combinations. Std-OIT specimens were extracted from different locations across the weld cross-section, including the HAZ, flashing, and bead (Figure 1).

Accepted manuscript doi:
10.1680/jgein.23.00178

Location 1 (Figure 1) was the exposed sheet material that was not affected by the welding. Location 2 (the heat-affected zone, HAZ_1) was sampled from the edge of the flashing adjacent to the weld track. Location 4 (the heat-affected zone, HAZ_2) was located at the sheet between the flashing and the weld bead. Location 5 was sampled from the extrudate bead. Location 3 was located at the flashing produced during the extrusion weld. The thickness of the bead/flashing was greater than that of the sheet. Additionally, the welding rod material had an average initial STD-OIT_o of 348 minutes, which was essentially double that of the sheet away from the weld. Thus, the Std-OIT depletion rate of the bead and flashing was slower than that of SAW (Figures 2, 3, and 4) for all examined welding parameter combinations. Despite the similarity in the depletion rate between HAZ_1 and the sheet material, the depletion rate of HAZ_2 was faster than that of the sheet for the Cool weld parameters (Figure 2).

For Good and Overheated welds, there was no significant difference between HAZ_1, HAZ_2, the flashing and the sheet material in depletion rate was observed (Figures 3 and 4). Thus, HAZ_1 did not experience enough exposure to heat to accelerate antioxidant depletion for all the examined welding parameters, whether this lack of acceleration was due to antioxidant depletion, morphological changes, or a combination of both (Francey and Rowe 2022a).

3.2 Melt Flow Index (MFI)

The molecular weight changes due to ageing were monitored using a high load melt flow index (HLMI) test. At 85°C, no change was observed in HLMI during the first 27 months of incubation for SAW (Figure 5). After 27 months, a reduction in the HLMI of sheet material was observed, and the normalized HLMI reached 0.6 after 40 months, suggesting the dominance of cross-linking oxidation reactions. No changes in HLMI were observed for the bead zone at 85°C during 40 months of immersion. This may be attributed to the longer time to depletion due to the higher initail OIT of the rod and greater thickness of the bead zone.

3.3 SCR performance

The SCR values of the notched sheet, unnotched sheet, and welds were monitored over 40 months in MSW-L3 at 85°C. For the sheet away from welding, early reduction in SCR values to the equilibrium stress crack resistance (SCR_m) due to physical ageing (Ewais and Rowe 2014; Rowe et al. 2019) was observed for the notched sheet at 85°C (Rowe et al. 2009). The mean SCR_m value was 616 ± 85 with SCR_m/SCR_0 = 0.64 (Table 1). During 27 months of immersion, thermo-oxidative degradation in SCR was observed for the notched sheet material. The time to nominal failure (t_{NF}) based on SCR can be assessed when SCR is reduced to 50% of SCR_m and observed after 30 months.

Accepted manuscript doi:
10.1680/jgein.23.00178

The unnotched sheet and weld specimens showed an exponential SCR reduction with incubation time (Figure 6). Thus, the data were plotted on a semi-log graph for analysis. The unnotched sheet SCR remained unchanged during the first 22 months of incubation at 85°C and then started to decrease (Figure 7). i The welds, including good welds, had a lower stress crack resistance than the unnotched sheet and remained at this value until the SCR of the unnotched sheet had reduced to a similar value as the good welds after about 27 months of incubation. At that time degradation in SCR of the good welds and of the notched sheet began. The S notched sheet reached a given SCR faster than t the unnotched sheet material. The difference is considered to represent the time required for craze formation, with the notch acting as a point of stress concentration, thereby hastening the rate of cracking (Abdelaal and Rowe 2015; Francey and Rowe 2022a). For the welds and unnotched sheet, a craze initiates in the weak zones at the welds and/or surface scratches and welds.

Prior to a decrease in SCR, good welds and many cool welds had in SCR between that of the notched and unnotched sheet. During this period, the eccentricity resulting from the welds (Giroud et al. 1995; Kavazanjian et al. 2017) accelerated the craze formation time relative to the unnotched sheet due to stress/strain concentration. This, is what is considered responsible for the lower SCR relative to the unnotched weld SCR failure time compared to the sheet.

Generally, welds show a similar change in behaviour to that of the notched sheet. The variation of unnotched SCR values for the three welding parameter combinations increased after 27 months of incubation. Some welds exhibit similar behaviour to the notched sheet material (Figure 8; Overheated), suggesting that material embrittlement can occur at the critical location (CRIT; location where the lower geomembrane sheet and the flashing intersect at the end of the weld; Figure 9; Rowe and Ali 2024) when preheat and barrel temperatures are high, resulting in high WIGI. The high variability in weld SCR over time was attributed to stress/strain concentration at the CRIT related to welding irregularities. Thus, the high-quality welds showed an unnotched SCR similar to that of the unnotched sheet, although the low-quality welds exhibited an unnotched SCR same as or below the notched sheet SCR.

Although there was a wide range in SCR for welds, most were between the SCR of the unnotched and notched sheet SCR failure time (Figure 7 and 8)) prior to degradation in SCR. Once degradation began, the SCR of the overheated welds were generally below that of the notched sheet. The time to nominal SCR failure (t_{NF}) for unnotched sheet was taken to be when the SCR value reached 250 hours (i.e. 50% of SCR required for new geomembrane by GRI GM 13) for the both the unnotched weld and sheet. The average t_{NF} for both Cool and Good welding parameter combinations was similar and equal to 34 months. The t_{NF} for the unnotched sheet was 37 months.

Accepted manuscript doi:
10.1680/jgein.23.00178

The t_{NF} for Overheated welds and the notched sheet was 31 months, suggesting that excessive heat may have facilitated welding irregularities (WIGI) contributing to this shorter t_{NF} due to the irregular geometry (WIGI) resulting in higher stress concentration and consequent accelerated craze formation in the CRIT zone of the weld. It was hypothesized that if stress concentration resulting from weld geometry irregularity (WIGI) were the primary factor controlling the difference in weld t_{NF}, a significant difference in weld SCR would be present and remain relatively constant at all ageing times. To quantify the welding irregularity, Rowe and Ali (2024) suggested the following equation to quantify the WIGI index, μ, in terms of the rotation of the upper sheet, extruded bead, and bottom sheet relative to the combined thickness of the bead and geomembrane located between flashing and bead zones (Figure 9).

$$\lambda = -0.182 \ln(\omega) - 0.5557 \quad (2)$$

$$\omega = \mu - \mu_0 \quad (3)$$

$$\mu = (\theta+\alpha) \times H/k \quad (4)$$

where λ is SCR/SCR_o; μ is WIGI index; θ is the angle between the horizontal line and the line between points a and b in radian; α is the angle between the horizontal line and the line between points b and c in radian; K is the bead thickness; H is the thickness between flashing and bead zone.

To examine the effect of WIGI on very aged specimens, Eq. 2 was applied to seven welding specimens immersed for 36 months at 85°C, each with a different WIGI index. The weld SCR was reduced by 92% when ω increased from 0.015 to 0.033 (Figure 10a). As already noted, this reduction was hypothesized to result from stress/strain concentration resulting from irregularities in weld geometry. When, Eq. 2 was applied to all unaged and aged specimens (Figure 10b), the results showed a similar effect of WIGI as was observed for the unaged specimens reported by (Rowe and Ali 2024).

Figure 11 shows two aged extrusion weld specimens' geometry with the same immersion time. When the specimen exhibited thickness at the area between flashing and extrudate bead (HAZ_2) similar to the lower sheet and had low eccentricity (ξ) between the centerline of the bead and the centerline of the lower sheet, the stress crack failure was located at CRIT adjacent to the flashing (Figure 11a). The stress crack failure was observed between flashing and bead when the thickness of HAZ_2 was less than the sheet and ξ was very high (Figure 11b). This occurred due to increased stress/strain concentration and faster AO depletion due to lower thickness (Figure 11).

Accepted manuscript doi:
10.1680/jgein.23.00178

3.4 Overground effect

HDPE geomembranes have low molecular weight oligomers that can bloom and form a waxy layer, preventing proper adhesion during welding. To ensure a successful extrusion weld, the geomembrane surface should be adequately ground to remove oxidized surfaces, dirt, dust, and additive blooms (Scheirs 2009). Excessive grinding beyond the welding zone reduces the geomembrane thickness adjacent to the welding zone, resulting in increased stress/strain concentration (Giroud et al. 1995). The examined overground weld specimens exhibited a reduction in the thickness ranges between 16 to 33% of the sheet material. All unaged and aged overground welds (Overheated or Normal) showed an SCR lower than that of notched sheets (Figure 12). Consequently, the t_{NF} for overground welds was shorter than that for the unnotched sheet, notched sheet, and well-grounded welds because the craze formation was accelerated in the overground zone (lower thickness relative to the sheet thickness) due to the stress concentration and faster degradation.

3.5 Results comparison between extrusion with fusion welds for MwA-15

Fusion welds were created using a DemTech pro-wedge series wedge welder by an experienced welding technician at a sheet temperature of 21°C. Three fusion welding scenarios were examined (denoted as "MwA#1; appropriate applied heat", "MwA#2; high applied heat", and "MwA#3; low heat required for welding flat die geomembranes"). MwA#1 welding cases had a wedge temperature T_w = 360°C and speed S = 2.6 m/min. MwA#2 welding cases had T_w = 460°C and S = 1.8 m/min. Finally, the MwA#3 welding case had T_w = 400°C and S = 3 m/min (Scheirs 2009; Francey and Rowe 2022b). These fusion weld samples were immersed in simulated MSW leachate at 85°C for 40 months and were periodically sampled.

SCR values for all unaged and aged fusion welded SCR specimens are plotted on the same graph as the unnotched SCR specimens of extrusion welds (Figure 13). The degradation of fusion and extrusion welds exhibited the same SCR general degradation behaviour. Thus, there is no statistically significant difference between the fusion and extrusion welds for either the unaged and similarly aged specimens. The stress concentration was attributed to welding geometry irregularity for extrusion welds (Rowe and Ali 2024) and/or adherence of squeeze-out beads for fusion welds, as illustrated in Figure 14 (Francey and Rowe 2022b). MwA#1 and MwA#2 exhibited inconsistent adherence to squeeze-out, leading to variations in failure locations based on the degree of squeeze-out adherence (Figure 14). Similarly, the Cool and Good welds exhibited inconsistent welding geometry due to low-quality control resulting from the high pressure applied by the operator. Overheated extrusion and fusion welds generally displayed shorter SCR failure times than the unnotched sheet material and

similar to the notched sheet (Figure 15), suggesting that the adherence of squeeze-out (fusion welds) and high WIGI (extrusion welds) may have accelerated craze formation compared to non-adhered squeeze-out bead (fusion welds) and low WIGI (extrusion welds) after ageing.

3.6 Shear strength properties

The mechanical properties of extrusion welds were assessed using a shear test in accordance with ASTM (D6392). Shear elongation is an essential parameter for evaluating the ductility of the welds, as it directly influences their longevity. The specimen was gripped at a distance of 25 mm from each side of the starting point of the weld bond, as specified by ASTM (D6392). The test was performed at a strain rate of 50 mm/min on high WIGI and low WIGI weld specimens aged for 36 months at 85°C. High WIGI resulted in a reduction in the break shear elongation (Figure 16). Both welds start to yield at 10 mm elongation, followed by a plateau phase at around 20mm for High WIGI and 30mm for Low WIGI welds. The break elongation for the low WIGI specimen (≈ 250 mm) was 1.55 times the high WIGI weld break elongation (≈150 mm). The reduction is attributed to the High WIGI that resulted in stress concentration at CRIT, initiating the rupture of the specimens at this point (Figure 17). No strain hardening was observed for either weld type. Thus, the shear test on extrusion weld may give insights into the critical locations (i.e., high WIGI).

3.7 Practical implications

The extrusion welds with Good temperature and low WIGI exhibited a similar unnotched SCR degradation behaviour as the appropriate fusion welding parameter combination. However, operator-induced irregularities resulting in high WIGI were more likely to occur in overheated welds, which could reduce the aged SCR and cause these welds to behave similarly to notched sheet and overheated fusion welds and resulted in a reduction in aged SCR by a factor of 10, indicating that more attention should be paid to the geometric irregularities (WIGI) of extrusion welds and avoiding overheated welding parameters. Thus, these welds should not be acceptable, even if they pass standard tests. The reduction in shear strength properties may provide insight into the critical locations along the extrusion welds, such as those with high WIGI. Extrusion welds exhibiting surface overgrinding adjacent to the flashing resulted in SCR lower than those of the notched sheet and faster t_{NF} relative to the sheet during incubation in MSW-L3. Abdelaal et al. (2014a) examined the brittle failure of 1.5 HDPE geomembranes under simulated landfill conditions using a Geosynthetic Liner Longevity Simulator (GLLS). They emphasized the significance of having a low notched sheet SCR value on brittle rupture in geomembranes subjected to gravel indentations. Aged geomembrane sheets pre-aged to a notched SCR of 75 hours exhibited brittle failure, corresponding to 35,000 holes per hectare when tested at 55°C. The number of holes per hectare increased at higher temperatures. Furthermore, the sheet material exhibited brittle ruptures at strains as low as 6% around individual gravel indentations.

Accepted manuscript doi:
10.1680/jgein.23.00178

In this study, after 36 months of immersion, MwA-15 displayed a notched SCR of 75 hours and an unnotched sheet SCR ≈ 7 times higher, around 500 hours. Good and Cool welds reached a similar unnotched SCR value of 500 hours after ≈ 29-32 months of immersion. Overheated welds reached that SCR failure time after about 28 months. Given the potential significance of a 75-hour notched sheet SCR for this material, welds may become susceptible to brittle rupture when exposed to strains of 6% after 28 months of incubation. Kavazanjian et al. (2017) found that with an average strain of 3%, there were maximum strains adjacent to the welds ranging from 2.3 to 4.0 times the average specimen strain. This suggests that the average strain adjacent to the welds only needs to be within the range of 1.5% to 2.6% to meet the 6% limit proposed by Abdelaal et al. (2014a). This finding atds further support to existing recommendations to avoid fusion or extrusion welds in high-strain zones (i.e., perpendicular to slopes or parallel to rigid structures). Additionally, during routine inspections, Construction Quality Assurance (CQA) should identify and reject welds with high WIGI, visible scratches or defects in the heat-affected zone (HAZ) adjacent to the flashing of extrusion welds, and any signs of surface overgrinding in CRIT (adjacent to flashing).

4. Conclusions

This study examined the long-term behaviour of SCR reduction and Std-OIT depletion of extrusion welds and 1.5 mm thick HDPE geomembrane sheets, using three different parameter combinations of welding (preheat and barrel temperatures) created by an experienced welding technician. Both aged and unaged SCR specimens were analyzed and discussed. The results provide insights into the t_{NF} concerning the unnotched SCR of both extrusion welds and sheet material and the notched SCR of the sheet material. They also highlight the role of weld-induced geometric irregularity (WIGI) in extrusion welds. Based on the extrusion welds and geomembrane examined in this paper, the following conclusions were reached.

1. The Std-OIT depletion of the sheet was similar to that of the heat-affected zones (HAZ_1) located adjacent to the flashing, while the area between the flashing and the bead (HAZ_2) may exhibit a faster or similar depletion rate compared to the sheet. This was attributed to the reduced thickness resulting from the high welding pressure applied by the operator.
2. There was no statistically significant difference between the SCR degradation behaviour of fusion and extrusion welds for Good welding parameters combination.
3. Overheated fusion and extrusion welds behave similarly to the notched sheet in terms of stress crack resistance degradation rate due to the high-stress concentration resulting from the high WIGI (in extrusion welds) and squeeze-out adherence (in fusion welds).

4. At the SCR failure time of 250 hours, the time to nominal failure (t_{NF}) for the notched sheet, unnotched sheet, Cool welds, and Good welds were 31 months, 37 months, 34 months, and 34 months, respectively. The t_{NF} of unnotched Overheated welds was equal to that of the notched sheet.
5. Overground welds exhibited a faster SCR degradation rate compared to that of the notched sheet due to stress concentration and accelerated degradation resulting from the reduced thickness.

This study only examined extrusion and fusion welds for one geomembrane. However, the results suggest that CQA should routinely identify and reject overheated, high WIGI extrusion welds, extrusion welds with notable scratches/defects in the HAZ adjacent to flashing, and welds with overground surfaces adjacent to flashing.

Data Availability Statement

Some or all data, models, or code that support the findings of this study are available from the corresponding author upon reasonable request.

Acknowledgments

The research presented in this paper was supported by the Natural Sciences and Engineering Council of Canada (NSERC Discovery Grant RGPIN/03928-2022 and the Geosynthetic Institute (GSI) fellowship grant). The equipment used was provided by funding from the Canada Foundation for Innovation (CFI) and the Government Ontario's Ministry of Research and Innovation.

List of notation

Basic SI units are shown in parentheses.

OIT_0 initial OIT value for unaged geomembrane (s)
OIT_t OIT value at time *t* (s)
s antioxidant depletion rate (s^{-1})
SCR_0 initial stress crack resistance value for unaged geomembrane (s)
SCR_m thermodynamically stable SCR value based on morphological change (s)
Std-OIT standard oxidative induction time (s)
H HAZ thickness at point "b (intersection point between bead and HAZ_2" (m)
K bead thickness at point "c (at the centerline of the bead) (m)
θ the angle between the horizontal line and the line between points "a" (centerline of the sheet at HAZ_1) and "b" (radians)
ω WIGI index (dimensionless)
λ normalized SCR (dimensionless)
ξ eccentricity between the centerline of the bead and the centerline of the lower sheet (dimensionless)
α angle between the horizontal line and the line between points b and c (radians)
t_{NF} time to nominal failure (s)
T_p preheat temperature (°C)
T_e barrel temperature (°C)
μ_0 WIGI index at low welding irregularity = 0.032 (dimensionless)

Abbreviations

ASTM	American Society for Testing and Materials
CQA	construction quality assurance
CRIT	critical location for weld stress cracking
GMB	geomembrane
GRI-GM13	standard specifications issued by GRI for testing and properties of HDPE GMBs
GLLS	geosynthetic Liner Longevity Simulator
HAZ	heat affected zone
HAZ_1	heat-affected zone located adjacent to the flashing
HAZ_2	Heat-affected zone located between the flashing and extrudate bead
HDPE	high-density polyethylene
HLMI	high load melt index
MSW	municipal solid waste
MFI	melt flow index
NCTL	notched constant tensile load
SAW	sheets away from the weld
SCR	stress crack resistance
WIGI	welding-induced geometric irregularity

References

Abdelaal, F.B., Morsy, M.S., Rowe, R.K., 2019. Long-term performance of a HDPE geomembrane stabilized with HALS in chlorinated water. Geotext Geomembranes 47, 815-830.

Abdelaal, F.B., Rowe, R.K., 2015. Durability of Three HDPE Geomembranes Immersed in Different Fluids at 85 degrees C. J Geotech Geoenviron 141.

Abdelaal, F.B., Rowe, R.K., Brachman, R.W.I., 2014a. Brittle rupture of an aged HPDE geomembrane at local gravel indentations under simulated field conditions. Geosynth Int 21, 1-23.

Abdelaal, F.B., Rowe, R.K., Islam, M.Z., 2014b. Effect of leachate composition on the long-term performance of a HDPE geomembrane. Geotext Geomembranes 42, 348-362.

Ali, M.M., Rowe, R.K., 2023. Effect of aged geomembrane extrusion welding on antioxidant depletion, Geosynthetics: Leading the Way to a Resilient Planet.

ASTM, 2019. D3895 Standard test method for oxidative induction time of polyolefins by differential scanning calorimetry. American Society for Testing and Materials, West Conshohocken, Pennsylvania, USA.

ASTM, D1238. Standard Test Method for Melt Flow Rates of Thermoplastics by Extrusion Plastometer. American Society for Testing and Materials. West Conshohocken, Pennsylvania, USA.

ASTM, D3895. Standard test method for oxidative induction time of polyolefins by differential scanning calorimetry. American Society for Testing and Materials, West Conshohocken, Pennsylvania, USA.

ASTM, D5397. Standard Test Method for Evaluation of Stress Crack Resistance of Polyolefin Geomembranes using Notched Constant Tensile Load Test. ASTM International, West Conshohocken, PA,USA.

ASTM, D6392. Standard Test Method for Determining the Integrity of No reinforced Geomembrane Seams Produced Using Thermo-Fusion Methods, Annual Book of ASTM Standards.

ASTM, D6693. Standard Test Method for Determining Tensile Properties of Nonreinforced Polyethylene and Nonreinforced Flexible Polypropylene. ASTM International, West Conshohocken, PA, USA.

Chappel, M.J., Rowe, R.K., Brachman, R.W.I., Take, W.A., 2012. A comparison of geomembrane wrinkles for nine field cases. Geosynth Int 19, 453-469.

Di Battista, V., Rowe, R.K., 2020. TCE and PCE diffusion through five geomembranes including two coextruded with an EVOH layer. Geotext Geomembranes 48, 655-666.

Ewais, A.M.R., Rowe, R.K., 2014. Effect of aging on the stress crack resistance of an HDPE geomembrane. Polym Degrad Stabil 109, 194-208.

Ewais, A.M.R., Rowe, R.K., Scheirs, J., 2014. Degradation behaviour of HDPE geomembranes with high and low initial high-pressure oxidative induction time. Geotext Geomembranes 42, 111-126.

Francey, W., Rowe, R.K., 2022a. Long-term stress crack resistance of HDPE fusion seams aged at 85?C in synthetic leachate. Can Geotech J.

Francey, W., Rowe, R.K., 2022b. Stress crack resistance of unaged high-density polyethylene geomembrane fusion seams. Geosynth Int.

Francey, W., Rowe, R.K., 2023. Importance of thickness reduction and squeeze-out Std-OIT loss for HDPE geomembrane fusion seams. Geotext Geomembranes 51, 30-42.

Gilson-Beck, A., Giroud, J.P., 2022. A quantification of the short-term reliability of HDPE geomembrane seaming methods. Geosynth Int.

Giroud, J.P., Tisseau, B., Soderman, K., Beech, J., 1995. Analysis of strain concentration next to geomembrane seams. Geosynthetics International, 2, No. 6, 1049–1097.

GRI-GM, 5(c). Seam Constant Tensile Load (SCTL) Test for Polyolefin Geomembrane Seams, Geosynthetic Research Institute, Drexel, PA, USA.

Hsuan, Y.G., 2000. Data base of field incidents used to establish HDPE geomembrane stress crack resistance specifications. Geotext Geomembranes 18, 1-22.

Hsuan, Y.G., Koerner, R.M., 1998. Antioxidant depletion lifetime in high density polyethylene geomembranes. J Geotech Geoenviron 124, 532-541.

Kavazanjian, E., Andresen, J., Gutierrez, A., 2017. Experimental evaluation of HDPE geomembrane seam strain concentrations. Geosynth Int 24, 333-342.

Mollard, S.J., Jefford, C.E., Staff, M.G., Browning, G.R.J., 1996. Geomembrane landfill liners in the real world, Geological Society, London, Engineering Geology Special Publications 1996, 11, 165-170.

Morsy, M.S., Rowe, R.K., 2020. Effect of texturing on the longevity of high-density polyethylene (HDPE) geomembranes in municipal solid waste landfills. Can Geotech J 57, 61-72.

Peggs, I.D., Carlson, D.S., 1990a. Brittle-Fracture in Polyethylene Geomembranes. Geosynthetics : Microstructure and Performance 1076, 57-77.

Rowe, R.K., Ali, M.M., 2024. Effect of welding parameters on properties of HDPE geomembrane extrusion welds. Geotext. Geomem. Https://doi.org/10.1016/j.geotexmem. 2023. 12.002.

Rowe, R.K. and Islam, M.Z. 2009. “Impact on landfill liner time-temperature history on the service-life of HDPE geomembranes”, Waste Management, 29(10):2689-2699.

Rowe, R.K., Sangam, H.P., 2002. Durability of HDPE geomembranes. Geotext Geomembranes 20, 77-95.

Rowe, R.K., Shoaib, M., 2017. Long-term performance of high-density polyethylene (HDPE) geomembrane seams in municipal solid waste (MSW) leachate. Can Geotech J 54, 1623-1636.

Rowe, R.K., Shoaib, M., 2018. Durability of HDPE Geomembrane Seams Immersed in Brine for Three Years. J Geotech Geoenviron 144.

Rowe, R.K and Yu, Y. 2019. Magnitude and significance of tensile strains in geomembrane landfill liners, Geotext. Geomembr., 47(3):429-458.

Rowe, R.K., Hsuan, Y.G., Lake, C.B., Sangam, P., Usher, S., 1998. Composite liner for a lagoon after 14 years of use.Proceedings of the Sixth International Conference on Geosynthetics, Vol.1, Atlanta, March.Industrial Fabric Association International, St Paul, MN, USA, pp.191–196.

Rowe, R.K., Islam, M.Z., Hsuan, Y.G., 2008. Leachate chemical composition effects on OIT depletion in an HDPE geomembrane. Geosynth Int 15, 136-151.

Rowe, R.K., Rimal, S., Sangam, H., 2009. Ageing of HDPE geomembrane exposed to air, water and leachate at different temperatures. Geotext Geomembranes 27, 137-151.

Rowe, R.K, Islam, M.Z. and Hsuan, Y.G. 2010. Effect of thickness on the ageing of HDPE geomembranes" ASCE *J Geotech. Geoenviron.*, 136(2):299-309

Rowe, R.K., Islam, M.Z., Brachman, R.W.I., Arnepalli, D.N. and Ewais, A.R. 2010. Antioxidant depletion from an HDPE geomembrane under simulated landfill conditions, ASCE *J Geotech. Geoenviron.*, 136:(7):930-939.

Rowe, R.K., Morsy, M.S., Ewais, A.M.R., 2019. Representative stress crack resistance of polyolefin geomembranes used in waste management. Waste Manag 100, 18-27.

Sangam, H.P. and Rowe, R.K 2005 Effect of surface fluorination on diffusion through an HDPE geomembrane. ASCE J Geotech. Geoenviron., 131(6):694-704.

Scheirs, J., 2009. A Guide to Polymeric Geomembranes: A Practical Approach, John Wiley & Sons, West Sussex, UK.

Seeger, Muller, 2003. Theoretical approach to designing protection: selecting a geomembrane strain criterion, Proceedings of the 1st IGS UK Chapter National Geosynthetics Symposium Held at The Nottingham Trent University on 17 June 2003, Dixon, N. Editor, Thomas Telford Publishing, London, UK, pp. 137–151.

Take, W.A., Chappel, M.J., Brachman, R.W.I. and Rowe, R.K. 2007. Quantifying geomembrane wrinkles using aerial photography and digital image processing, Geosynth. Int., 14(4):219-227.

Toepfer, G.W., 2015. Extrusion seams – the good, the bad, and the ugly, Geosynthetics Conference Proceedings, Portland, OR, USA, pp. 108–117.

Tognon, A.R., Rowe, R.K. and Moore, I.D. 2000. Geomembrane strain observed in large-scale testing of protection layers, ASCE *J Geotech. Geoenviron.*, 126(12):1194-1208.

Touze-Foltz, N., Lupo, J., Barroso, M., 2008. Geoenvironmental applications of geosynthetics, Keynote Lecture. Proc Eurogeo 4, 98 the 4th European Conference on Geosynthetics, Edinburgh, Scotland, UK.

Zhang, L., Bouazza, A., Rowe, R.K., Scheirs, J., 2017. Effect of welding parameters on properties of HDPE geomembrane seams. Geosynth Int 24, 408-418.

Accepted manuscript doi:
10.1680/jgein.23.00178

Table 1. Initial properties of the HDPE geomembrane (GMB) examined.

Properties	Method	Unit	GMB1
Nominal thickness	ASTM D 5199	mm	1.5
Geomembrane designation			MwA-15
Manufacturing date			2011
Manufacturing technique			Flat die
Standard oxidative induction time (Std-OIT)	ASTM D 3895	min	165 ± 2
High-pressure oxidative induction time (HP-OIT)	ASTM D 5885	min	1321 ± 12
Suspected HALS			Yes
HLMI (21.6 kg/190 ℃)	ASTM D 1238	g/10 min	21.5 ± 0.2
SCR	ASTM D 5397	hours	1012 ± 85
SCR_m	ASTM D5397	Hours	616 ± 58
Yield stress for SCR		kN/m	29.3
Tensile yield strength (MD)	ASTM D 6693 Type (IV)	kN/m	29.6 ± 0.5
Tensile yield strain (MD)		%	19.7 ± 0.3
Tensile break strength (MD)		kN/m	46.4 ± 0.3
Tensile break strength (MD)		%	760 ± 13.8

Table 2. Constituents of synthetic leachate used for immersion tests.

Inorganics		
Chemical	Formula	Concentration (mg/L, except where noted)
Sodium Hydrogen Carbonate	$NaHCO_3$	3012
Calcium Chloride	$CaCl_2•H_2O$	2882
Magnesium Chloride	$MgCl_2•6H_2O$	3114
Magnesium Sulfate Heptahydrate	$MgSO_4•7H_2O$	319
Ammonium Hydrogen Carbonate	NH_4HCO_3	2439
Urea	$CO(NH_2)_2$	695
Sodium Nitrate	$NaNO_3$	50
Potassium Carbonate	K_2CO_3	324
Potassium Hydrogen Carbonate	$KHCO_3$	312
Potassium dihydrogen phosphate	K_2HPO_4	30
Trace metals		
Chemical	Formula	Concentration (mg/L, except where noted)
Ferrous sulfate heptahydrate	$FeSO_4•7H_2O$	2000
Boric Acid	H_3BO_3	50
Zinc sulfate heptahydrate	$ZnSO_4•7H_2O$	50
Copper sulfate pentahydrate	$CuSO_4•5H_2O$	40
Manganese sulfate	$MnSO_4•H_2O$	500
Ammonium heptamolybdate tetrahydrate	$(NH_4)_6Mo_7O_{24}•4H_2O$	50
Aluminium Sulfate Hexadecahydrate	$Al_2(SO_4)_3•16H_2O$	30
Cobalt sulfate heptahydrate	$CoSO_4•7H_2O$	150
Nickel sulfate hexahydrate	$NiSO_4•6H_2O$	500
Sulfuric acid. (mL/L)	H_2SO_4	1
Surfactant Igepal CA720 (mL/L)	$(C_2H_4O)_nC_{14}H_{22}O$	5
Eh (adjusted by adding 3% w/v $Na_2S•9H_2O$) (mV)		120
pH (adjusted by adding either NaOH or H_2SO_4) (–)		6

* Rowe et al. (2008); Abdelaal et al. (2014)

Accepted manuscript doi:
10.1680/jgein.23.00178

Figure captions

Figure 1. Photography of the extrusion weld cross-section, showing locations of the sampling for the Std-OIT of extrusion welding showing the eight locations of testing

Figure 2. Extrusion weld zone Std-OIT depletion with ageing at 85°C for Cool welds, MwA#1 (Preheat/Barrel; 150°C/230°C).

Figure 3. Extrusion weld zone Std-OIT depletion with ageing at 85°C for Good welds, MwA#2 (Preheat/Barrel; 220°C/230°C).

Figure 4. weld zone Std-OIT depletion with ageing at 85°C for Overheated welds, MwA#3 (Preheat/Barrel; 277°C/288°C).

Figure 5. Variation in notched SCR for the sheet material and HLMI for the sheet material (SAW) and the bead zone incubated at 85°C. Error bars representing maximum and minimum failure times for the unnotched sheet.

Figure 6. Change in unnotched extrusion weld vs unnotched sheet SCR over time with ageing at 85°C. Error bars representing maximum and minimum failure times for the unnotched sheet.

Figure 7. Variation in unnotched extrusion weld SCR (Cool welds (Preheat/Barrel; 150°C/230°C) and Good (Preheat/Barrel; 220°C/230°C) compared to notched and unnotched sheets SCR over time with ageing at 85°C. Error bars representing maximum and minimum failure times for the unnotched sheet.

Figure 8. Variation in unnotched extrusion weld SCR (Overheated welds (Preheat/Barrel; 277°C/288°C) compared to notched and unnotched sheet SCR over time with ageing at 85°C. Error bars representing maximum and minimum failure times for the unnotched sheet.

Figure 9. Cross-section view of a typical high geometry irregularity (WIGI) extrusion weld specimen after failure in stress crack test.

Figure 10. Variation of λ versus ω for (a) aged extrusion welds GMBs specimens at 36 months ageing at 85°C (b) all data points (aged – unaged)

Figure 11. Images of brittle failure between the welding bead and the flashing area, and adjacent to welding flashing at 34 months ageing at 85°C due to welding irregularity (WIGI).

Figure 12. Variation in unnotched normal ground extrusion welds SCR compared to overground extrusion welds, notched sheet and unnotched sheet SCR over time with ageing at 85°C. Error bars representing maximum and minimum failure times for the unnotched sheet.

Figure 13. Variation in unnotched normally ground extrusion welds SCR compared to fusion welds and unnotched sheet SCR over time with ageing at 85°C. Error bars representing maximum and minimum failure times for the unnotched sheet.

Figure 14. Images of brittle failure between the welding bead and the flashing area, and adjacent to welding flashing at 34 months ageing at 85°C due to welding irregularity (WIGI).

Figure 15. Variation in unnotched extrusion welds SCR compared to fusion welds and unnotched sheet SCR over time with ageing at 85°C. Error bars representing maximum and minimum failure times for the unnotched sheet.

Figure 16. Shear Force versus elongation curves for Low WIGI and High WIGI overheated welds aged for 36 months at 85 °C.

Figure 17. Left to right: shear test specimen for High WIGI weld at failure, shear test specimen for Low WIGI weld at failure aged for 36 months at 85°C.

Accepted manuscript doi:
10.1680/jgein.23.00178

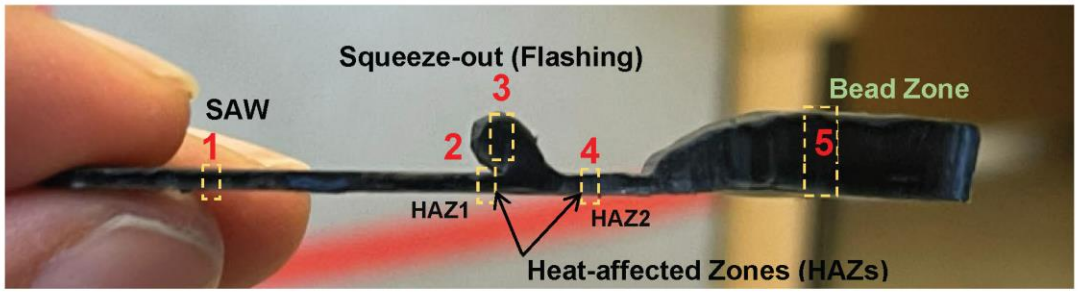

Figure 1

Accepted manuscript doi:
10.1680/jgein.23.00178

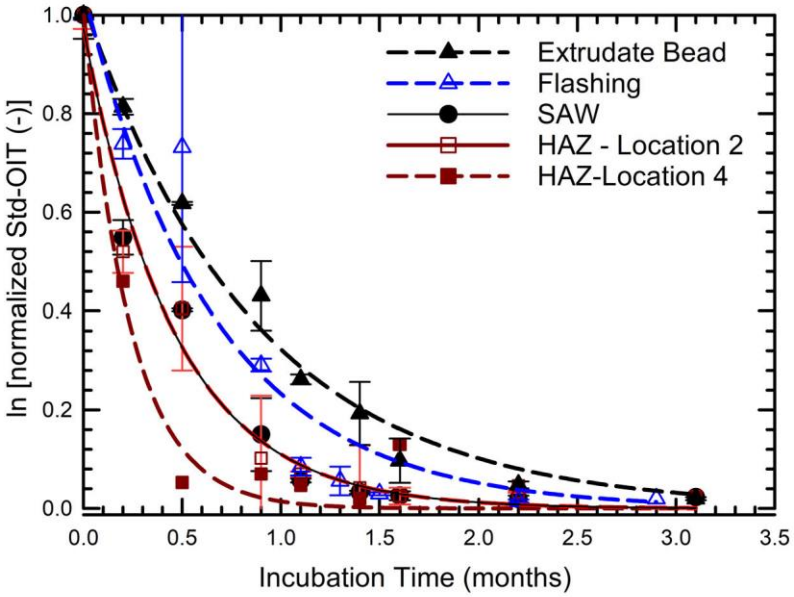

Figure 2

Accepted manuscript doi:
10.1680/jgein.23.00178

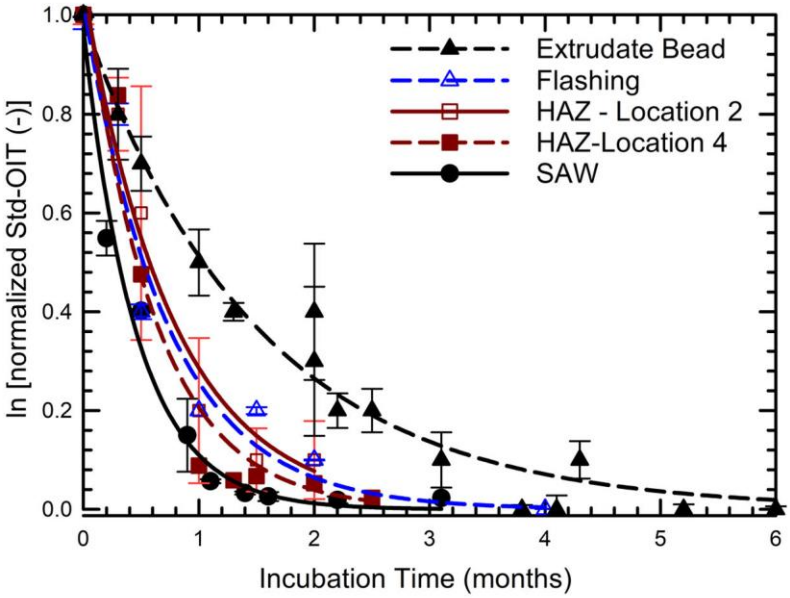

Figure 3

Accepted manuscript doi:
10.1680/jgein.23.00178

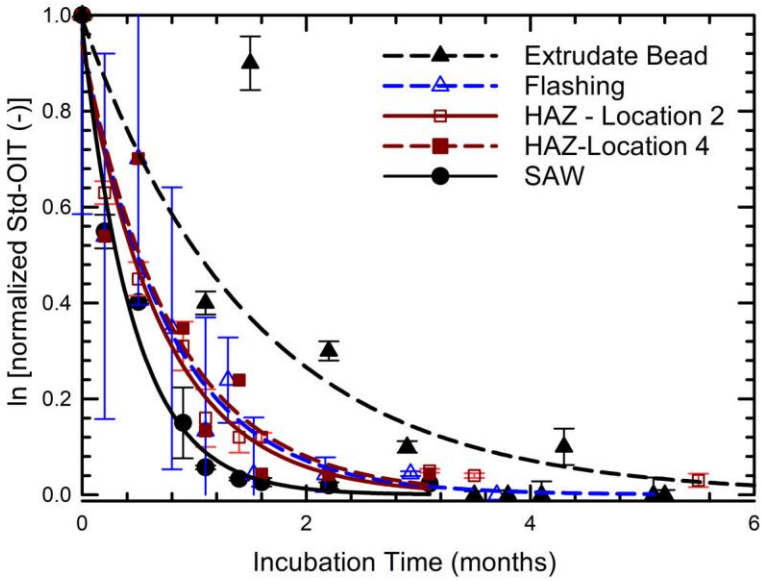

Figure 4

Accepted manuscript doi:
10.1680/jgein.23.00178

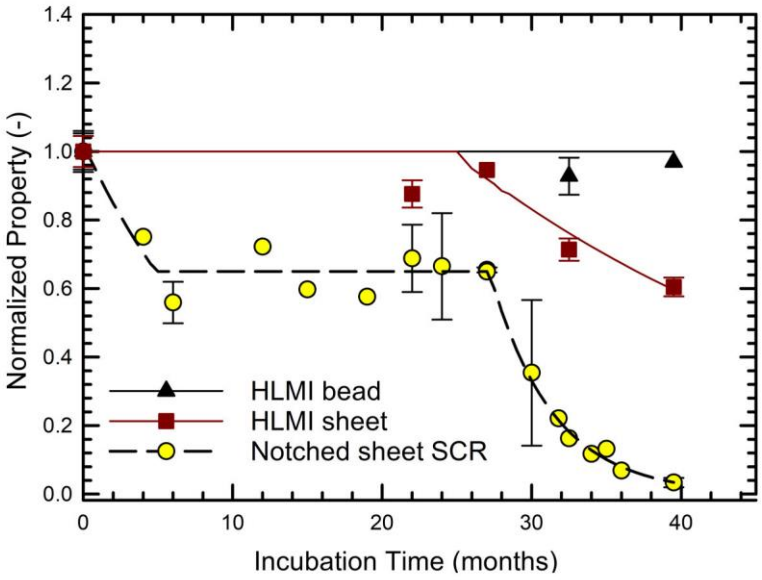

Figure 5

Accepted manuscript doi:
10.1680/jgein.23.00178

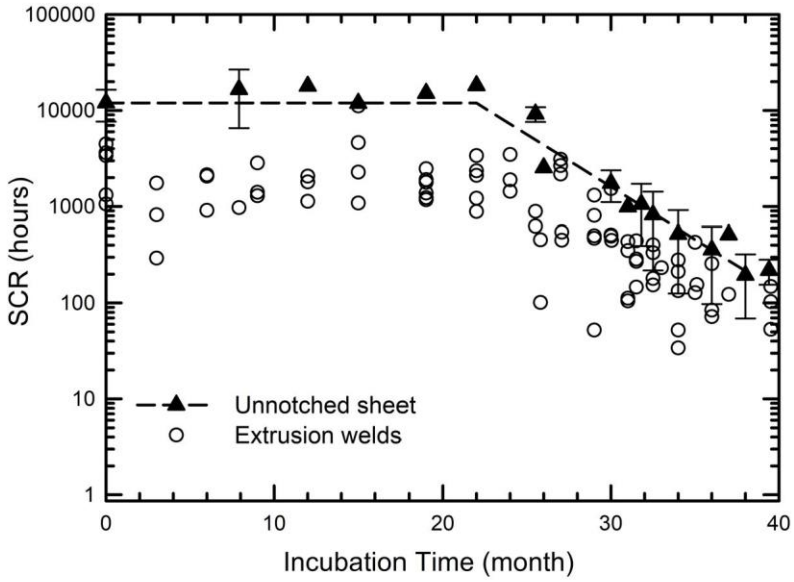

Figure 6

Accepted manuscript doi:
10.1680/jgein.23.00178

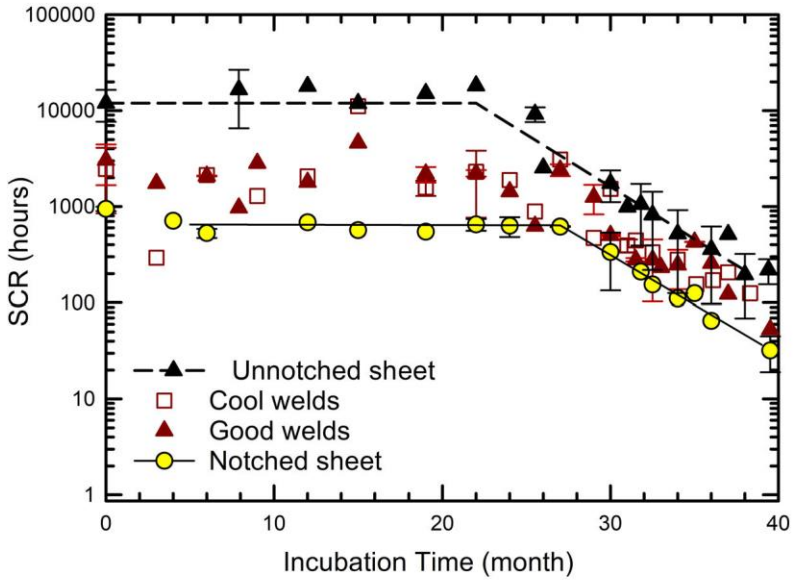

Figure 7

Accepted manuscript doi:
10.1680/jgein.23.00178

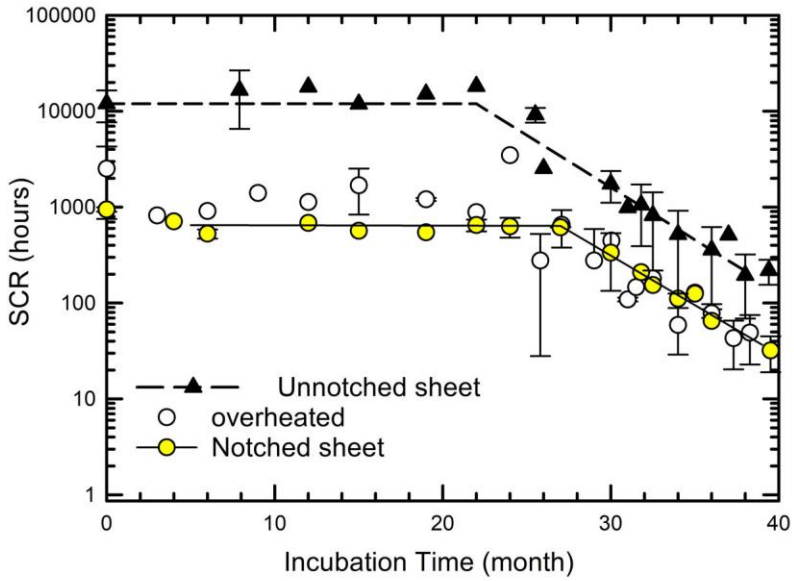

Figure 8

Accepted manuscript doi:
10.1680/jgein.23.00178

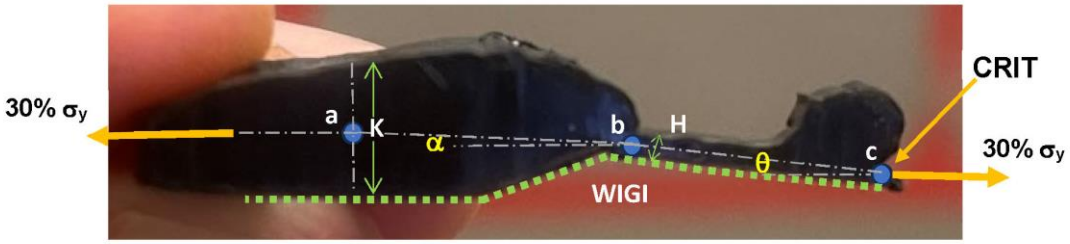

Figure 9

Accepted manuscript doi:
10.1680/jgein.23.00178

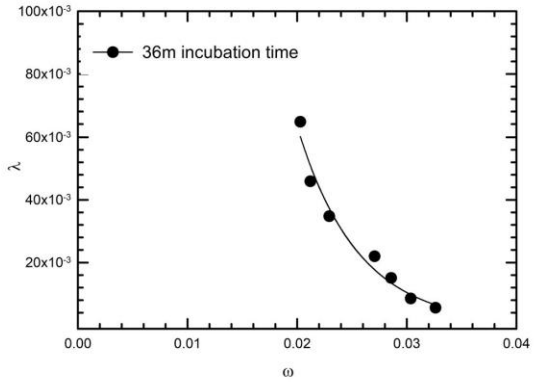

Figure 10a

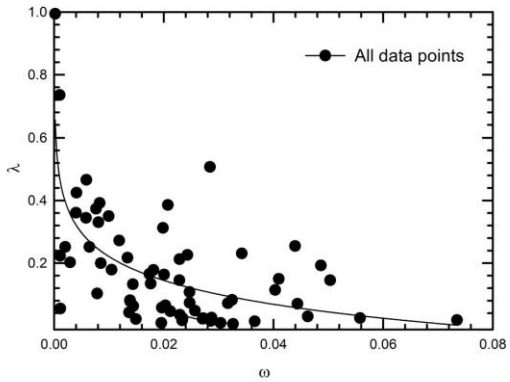

Figure 10b

Figure 10

Accepted manuscript doi:
10.1680/jgein.23.00178

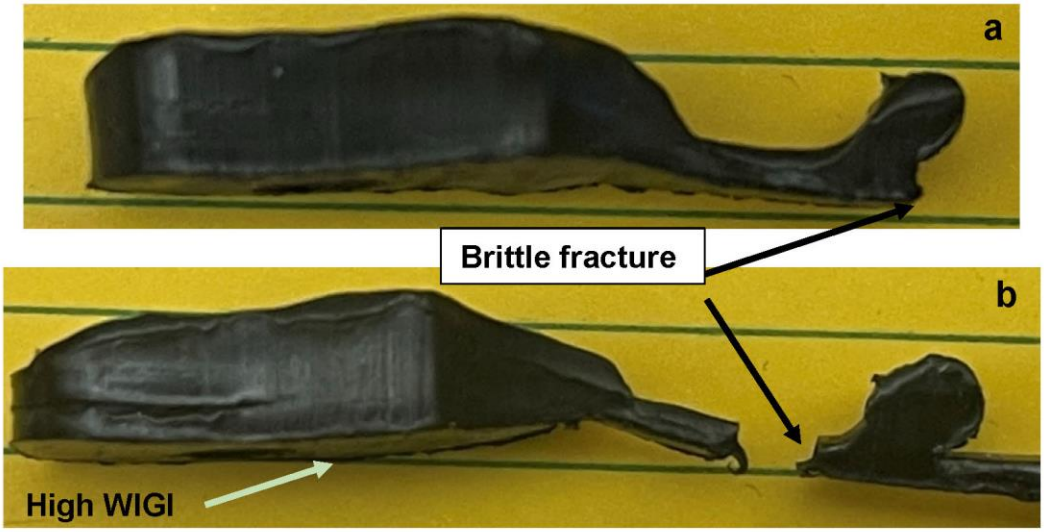

Figure 11

Accepted manuscript doi:
10.1680/jgein.23.00178

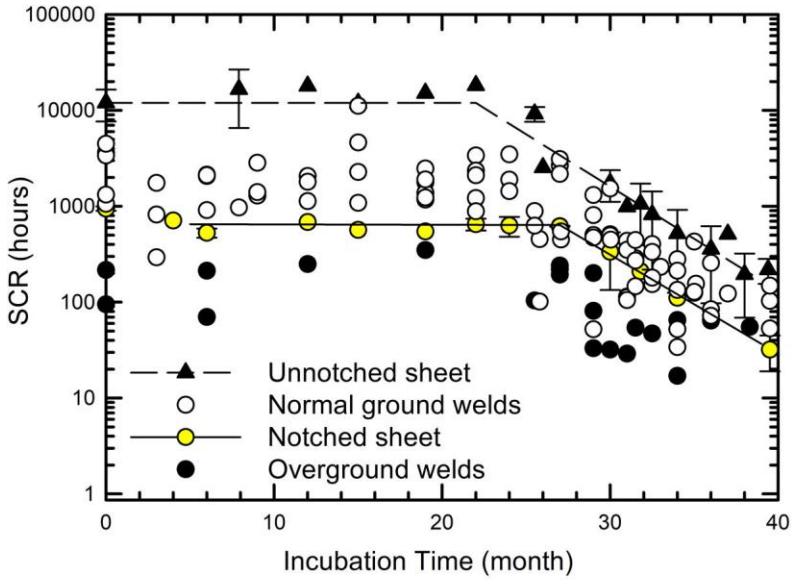

Figure 12

Accepted manuscript doi:
10.1680/jgein.23.00178

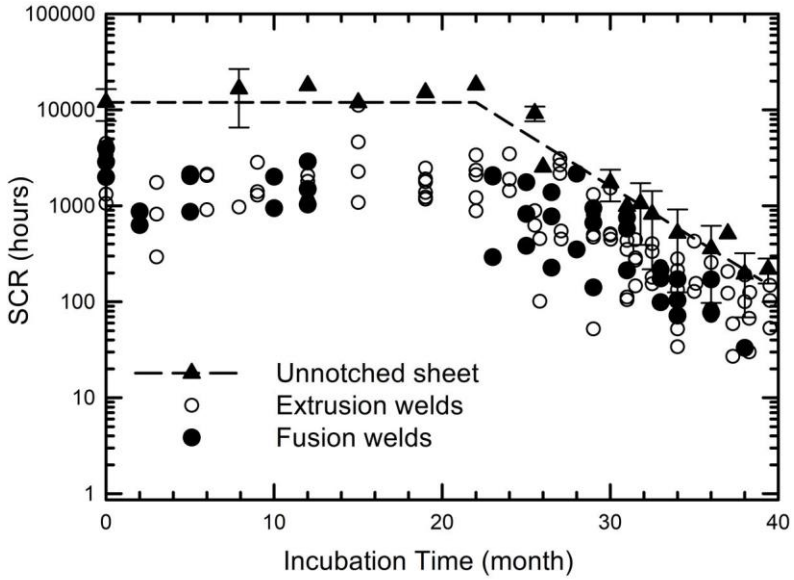

Figure 13

Accepted manuscript doi:
10.1680/jgein.23.00178

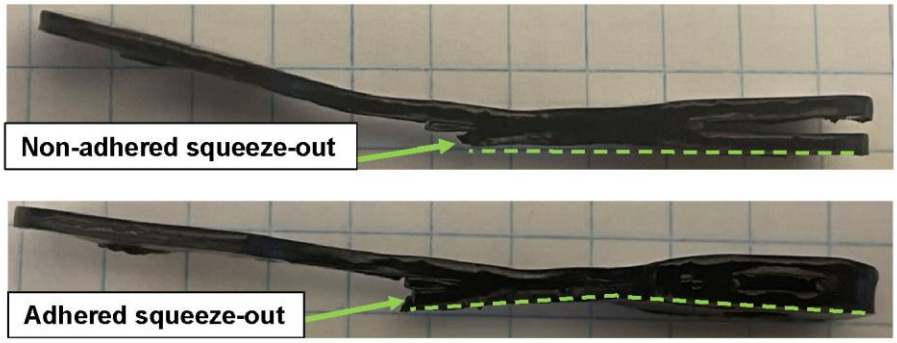

Figure 14

Accepted manuscript doi:
10.1680/jgein.23.00178

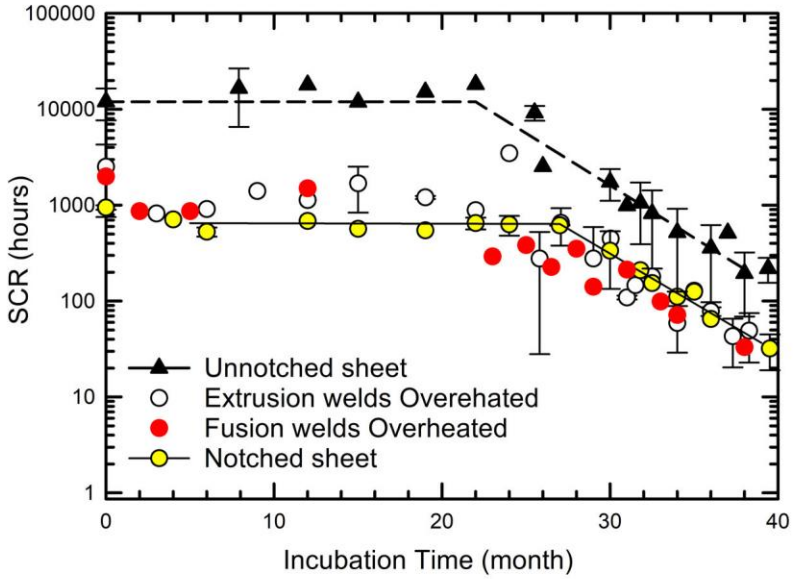

Figure 15

Accepted manuscript doi:
10.1680/jgein.23.00178

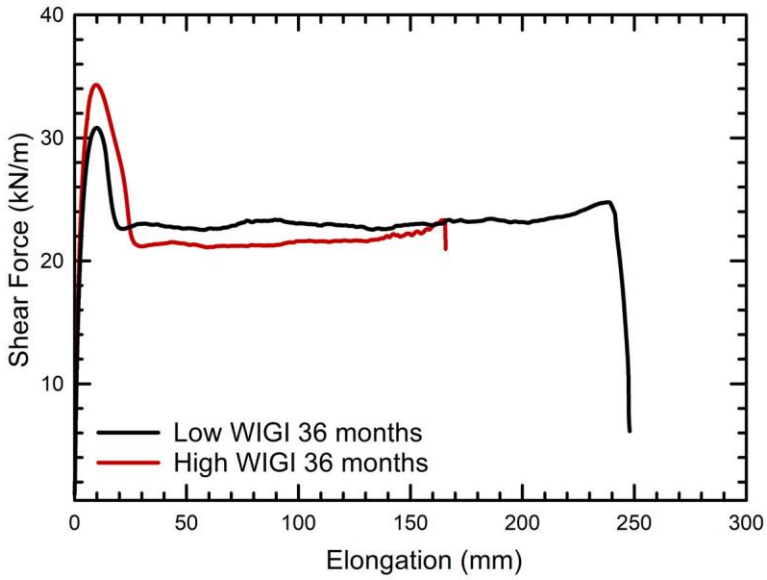

Figure 16

Accepted manuscript doi:
10.1680/jgein.23.00178

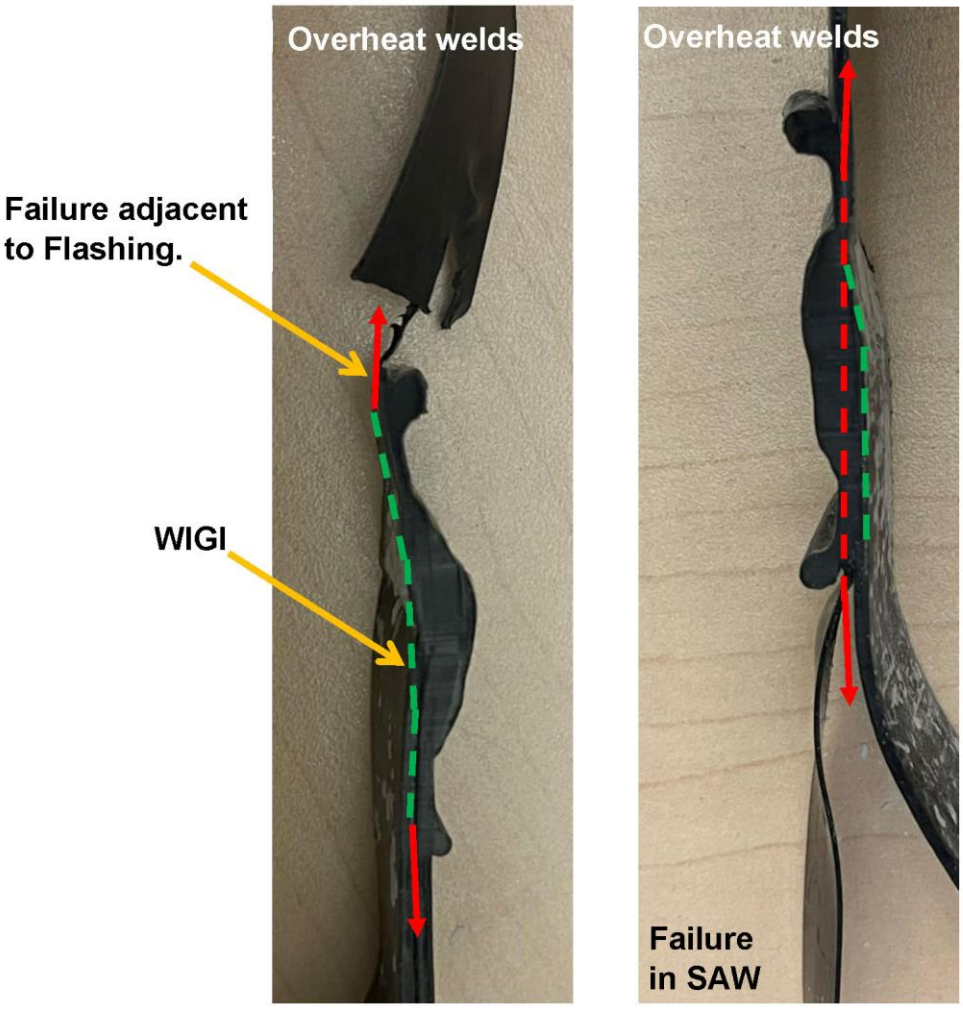

Figure 17